Journal of Catalysis 300 (2013) 251–259

Contents lists available at SciVerse ScienceDirect

Journal of Catalysis

journal homepage: www.elsevier.com/locate/jcat

Influence of extra-framework Al on the structure of the active iron sites in Fe/ZSM-35

Junying Wang [a,b], Haian Xia [a], Xiaohua Ju [a], Zhaochi Feng [a], Fengtao Fan [a], Can Li [a,*]

[a] State Key Laboratory of Catalysis, Dalian Institute of Chemical Physics, Chinese Academy of Sciences, 457 Zhongshan Road, Dalian 116023, China
[b] Graduate University of Chinese Academy of Sciences, Beijing 100049, China

ARTICLE INFO

Article history:
Received 25 October 2012
Revised 11 January 2013
Accepted 14 January 2013

Keywords:
Binuclear iron sites
Extra-framework Al
N_2O decomposition
Fe/ZSM-35
Raman spectroscopy

ABSTRACT

The influence of extra-framework Al via $AlCl_3$ deposition on the structure of the active Fe sites in Fe/ZSM-35 was investigated by ^{29}Si MAS NMR, UV–visible diffuse reflectance spectroscopy, infrared spectroscopy, UV Raman spectroscopy, and ^{57}Fe Mössbauer spectroscopy combined with catalytic decomposition of N_2O. It is found that high-temperature treatment considerably modifies the iron speciation. UV–visible diffuse reflectance spectra and in situ infrared spectra of NO adsorption show that a significant amount of clustered and cationic Fe species is transformed into extra-framework Fe–O–Al mixed oxide species by high-temperature treatment. UV Raman spectra and ^{57}Fe Mössbauer spectra suggest the generation of a binuclear Fe site stabilized by extra-framework Al species with a feature Raman band at 875 cm^{-1}, which is associated with the high activity of N_2O decomposition. A possible explanation is that the addition of extra-framework Al species is beneficial for the formation of binuclear active Fe sites bound to extra-framework Al.

1. Introduction

Fe/ZSM-35 catalysts have shown good catalytic activity for a number of reactions, such as selective reduction in NO_x by NH_3 or hydrocarbons [1,2], oxidation of benzene to phenol using N_2O [3], and N_2O decomposition [4–8]. Despite the exploration of their catalytic properties, much less attention has been paid to a detailed understanding of the structure of the active iron sites. On the basis of DFT calculations in combination with spectroscopic investigations, Sklenak and co-workers proposed that the active sites are composed of two Fe^{2+} cations coordinated in two adjacent six-membered rings of ferrierite [4,9]. Kachurovskya and Daturi assumed that Fe^{2+} ions located at the wall of the main (10-membered ring) ferrierite channel were the active sites for N_2O decomposition based on DFT calculations [10,11]. Very recently, our studies have shown that the active iron site for N_2O decomposition is an $Fe_2(\mu\text{-}O)$ site, giving a characteristic Raman band at 875 cm^{-1} using in situ UV resonance Raman spectroscopy combined with Mössbauer spectroscopy and DFT calculations [12]. Moreover, recent studies have revealed that the presence of Al pairs is responsible for the higher catalytic activity of Fe/FER in N_2O decomposition [13,14]. However, the role of the extra-framework Al species inevitably formed under pretreatment conditions remains elusive. Experimentally, it is a big challenge to distinguish the active iron species from those of abundantly present spectator iron species, since the active iron species usually account for only a small portion of the total iron content [4,10,13,15–17].

In this work, the effect of extra-framework Al species via $AlCl_3$ deposition on the structure of the active iron sites and the activity in N_2O decomposition was investigated by ^{29}Si MAS NMR, UV–visible diffuse reflectance spectroscopy, infrared (IR) spectroscopy, UV Raman spectroscopy, and ^{57}Fe Mössbauer spectroscopy. It is shown that high-temperature treatment and the extra-framework Al species via $AlCl_3$ deposition considerably modify the structure of the binuclear active Fe sites and profoundly increase the activity in direct N_2O decomposition.

2. Experimental

2.1. Catalyst preparation

Fe/ZSM-35 catalysts with different amounts of extra-framework Al were prepared by solid-state ion-exchange method [18–23]. Briefly, 2 g of NH_4/ZSM-35 sample (atomic ratio SiO_2/Al_2O_3 = 21, synthesized in our laboratory) was calcined at 823 K in a flow of O_2 for 2 h and ground with appropriate amounts of anhydrous $FeCl_3$ and/or anhydrous $AlCl_3$ in a glove box. The well-mixed powder was first heated in helium flow by raising the temperature from RT to 598 K and kept at 598 K for 2 h. Then, the sample was heated in 0.5 vol% H_2O/He flow at 473 K for 1 h to hydrolyze Fe–

* Corresponding author. Fax: +86 411 84694447.
E-mail address: canli@dicp.ac.cn (C. Li).
URL: http://www.canli.dicp.ac.cn (C. Li).

0021-9517/$ - see front matter © 2013 Published by Elsevier Inc.
http://dx.doi.org/10.1016/j.jcat.2013.01.011

Cl and Al–Cl bonds. Finally, the sample was calcined in a flow of O_2 at 823 K for 2 h to obtain Fe/ZSM-35-C (x) or Al/ZSM-35-C, where C refers to calcination in flowing O_2 at 823 K and x to atomic ratios of extra-framework Al/Fe. A portion of calcined Fe/ZSM-35-C (x) or Al/ZSM-35-C was further treated at 1173 K in pure helium flow for 2 h and refers to Fe/ZSM-35-HT (x) or Al/ZSM-35-HT, where HT denotes a high-temperature treatment.

2.2. Catalyst characterization

X-ray diffraction patterns (XRD) of Fe/ZSM-35 samples were recorded on a Rigaku Miniflex X-ray diffractometer equipped with a Cu Kα monochromatic radiation source (λ = 1.5418 Å). No bulky iron oxides were detected (not shown).

^{29}Si MAS NMR spectra were performed on a Varian Infinityplus-400 spectrometer, with a spinning rate of 6 kHz. Chemical shifts were obtained relative to 4,4-dimethyl-4-silapentane sulfonate sodium (DSS) as a reference. A total of 1304 scans were accumulated with a $\pi/2$ pulse width of 1.8 μs and a 4-s pulse delay.

UV–visible diffuse reflectance spectra (UV–visible DRS) were recorded on a JASCO V-550 spectrometer equipped with an integrating sphere coated with $BaSO_4$. The baseline was corrected using $BaSO_4$ as a reference material.

All IR spectra were collected on a FT-IR spectrometer (Nicolet Nexus 470) with a resolution of 4 cm^{-1} and 32 scans in the region 4000–650 cm^{-1}. All IR experiments were performed as follows: The sample was pressed into a self-supporting wafer (ca. 15 mg cm^{-2}) and put into a quartz IR cell equipped with CaF_2 windows. First, the calcined samples were pretreated in flowing oxygen at 623 K for 1 h, while the high-temperature treated samples were treated in helium flow at 623 K for 1 h. Then, the sample was cooled to room temperature in the same flow, followed by purging with helium for 30 min. A spectrum was collected as a reference. Subsequently, NO/He (1.0 vol%) was introduced onto the sample for NO adsorption at room temperature. After the sample was purged with helium for 30 min, the IR spectrum was recorded.

UV Raman spectra were recorded in situ on a homemade UV Raman spectrograph with a triple-stage spectrograph at a resolution of 2 cm^{-1}. The laser line at 325 nm emitted from a KIMMON IK-3351 R-G He–Cd laser was used as an exciting source. The power of the laser that reached the samples was about 1.0 mW. The samples were pressed into self-supporting wafers (~15 mg cm^{-2}) and put into an in situ quartz cell. The sample wafers were calcined at 823 K in flowing O_2 for 1 h. The high-temperature-treated sample wafers were first calcined at 823 K in a flow of O_2 for 1 h, followed by treatment at 1173 K in flowing He for 1 h. The in situ quartz Raman cell was closed and cooled to room temperature, and then, the spectra were recorded.

^{57}Fe Mössbauer spectra were measured at 78 K on a spectrometer working in the mode of constant accelerations with the use of a ^{57}Co: Rh source. Data analysis involved a least-square fitting procedure assuming a Lorentzian peak shape and employed the fitting program MössWin 3.0 i. The isomer shift (IS) values were given relative to iron foil at room temperature.

The transient-response method adopted by Kiwi-Minisker et al. [24] was applied for the determination of the concentrations of active Fe sites. In this method, 50 mg of a catalyst was placed into a quartz plug-flow reactor and pretreated at 1173 K in helium flow for 1 h, followed by cooling to 523 K in flowing helium. The reaction gas phase was continuously monitored in the reactor outlet after a quick switch from He flow to N_2O/He (5.0 vol%) flow. N_2O decomposition leads to the formation of gaseous N_2 and the deposition of an equal amount of surface oxygen species [24,25]. The quantity of active Fe sites was estimated by integration of the evolved N_2 peak based on the assumption that one oxygen atom was deposited on each Fe site [24].

2.3. Activity measurement

N_2O decomposition activity was tested for both calcined and high-temperature-treated Fe/ZSM-35 catalysts. The amount of a catalyst placed in a fixed-bed plug-flow reactor was about 50 mg. Before each run, the catalyst was pretreated at 823 K in flowing O_2 (Fe/ZSM-35-C) or at 1173 K in flowing helium (Fe/ZSM-35-HT) for 1 h and then cooled down to the reaction temperature. The feed gas composition was N_2O/He (5.0 vol%). The total gas flow was controlled by mass flow controllers and maintained at a GHSV of 24,000 h^{-1}. An online mass spectrometer (Gam 200, Pfeiffer Vacuum) calibrated by gas mixtures of known compositions was used for quantitative analysis of the gas-phase concentrations.

3. Results and discussion

3.1. ^{29}Si MAS NMR spectra of Fe/ZSM-35 samples

Fig. 1A and B show the ^{29}Si MAS NMR of Fe/ZSM-35 catalysts calcined at 823 K in O_2 and pretreated in helium at 1173 K, respectively. The NMR peaks at −115 and −112 ppm come from the $Si(OSi)_4$ groupings in ZSM-35 and the peak at −106 ppm reflects $Si(OAl)(OSi)_3$ [26]. The framework and extra-framework Al content is given in Table 1. Compared to Fe/ZSM-35-C (x = 0, 1, 2) samples, the extra-framework Al content increases significantly for Fe/ZSM-35-HT (x = 0, 1, 2) samples, suggesting that a large amount of Al was extracted from framework to extra-framework positions during high-temperature treatment.

3.2. Catalytic decomposition of N_2O

Fig. 2A and B present the dependence of N_2O conversion on the reaction temperature in direct N_2O decomposition for calcined and high-temperature-treated Fe/ZSM-35 samples. For the calcined Fe/ZSM-35 (x = 0, 1, 2) catalysts, the onset of the reaction occurs at approximately 663–683 K, and full N_2O conversion is reached at ca. 753–773 K, whereas N_2O decomposition starts at about 623–633 K and is completed at around 693–713 K for the catalysts treated in helium at 1173 K. Another point to note is that the activity in direct N_2O decomposition of both calcined and high-temperature-treated catalysts is in the same order: Fe/ZSM-35 (x = 2) > Fe/ZSM-35 (x = 1) > Fe/ZSM-35 (x = 0). A blank experiment on Al/ZSM-35 prepared by the same method as that for the Fe/ZSM-35 catalysts shows that the activity in N_2O decomposition is negligible, suggesting that the extra-framework Al species are not solely responsible for the decomposition of N_2O, and Fe is the active component for the formation of the active sites. The results provide a strong indication that high-temperature treatment has a great influence on the structure of the active iron sites, and the present extra-framework Al species have a promotional effect on the formation of the active Fe sites for N_2O decomposition.

Table 2 lists the apparent activation energies and apparent pre-exponential factors for both calcined and high-temperature-activated catalysts. These data were calculated from Arrhenius plots under the assumption that N_2O decomposition is an apparent first-order reaction. For the calcined catalysts, introduced extra-framework Al species slightly affect the apparent activation energy E_a, which decreases from 185 kJ mol^{-1} for Fe/ZSM-35 (x = 0) to 165 kJ mol^{-1} for Fe/ZSM-35 (x = 1) and to 169 kJ mol^{-1} for Fe/ZSM-35 (x = 2). This reflects the nature of iron sites for N_2O decomposition not being much changed in these samples. After the catalysts are treated in helium at 1173 K, the apparent activation energies increase to about 200 kJ mol^{-1} while the pre-exponential factors increase to the order of ~10^2–10^5. In a simplified kinetic analysis, the apparent pre-exponential factor A is the product of

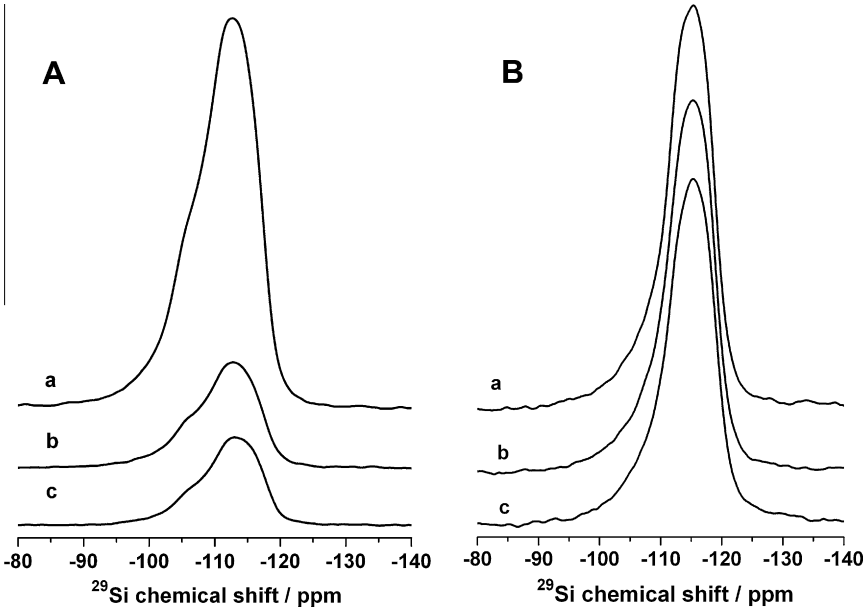

Fig. 1. ^{29}Si MAS NMR spectra of (A) calcined and (B) high-temperature-treated Fe/ZSM-35 catalysts: (a) Fe/ZSM-35 ($x = 0$), (b) Fe/ZSM-35 ($x = 1$), (c) Fe/ZSM-35 ($x = 2$).

Table 1
Al content, framework Si/Al ratios, and framework and extra-framework Al content in calcined and high-temperature-treated Fe/ZSM-35 catalysts.

Catalyst	Al[a] (wt.%)	Si/Al_{FR}[b]	Framework al species (wt.%)	Extra-framework Al species (wt.%)
Fe/ZSM-35-C ($x = 0$)	3.41	14.0	3.21	0.20
Fe/ZSM-35-C ($x = 1$)	3.65	14.2	3.17	0.48
Fe/ZSM-35-C ($x = 2$)	4.07	14.3	3.14	0.93
Fe/ZSM-35-HT ($x = 0$)	3.41	38.8	1.16	2.25
Fe/ZSM-35-HT ($x = 1$)	3.65	39.1	1.15	2.50
Fe/ZSM-35-HT ($x = 2$)	4.07	41.9	1.07	3.00

[a] Determined by ICP.
[b] Framework Si/Al ratios determined by ^{29}Si MAS NMR.

the number of active sites and the kinetic pre-exponential factor, which is the ratio of the partition functions of the transition state excluding that of the reaction coordinate and that of the ground state. Thus, the large difference in pre-exponential factors between the calcined and high-temperature-treated samples indicates that the number of active iron sites is remarkably changed during high-temperature activation. The higher apparent activation energies suggest that the nature of the active iron sites changes. However, the higher apparent activation energies are compensated for by the higher pre-exponential factors, which leads to extremely high activity of the Fe/ZSM-35-HT ($x = 0, 1, 2$) samples. To confirm this hypothesis, $\ln A$ is then plotted against E_a for the high-temperature-treated Fe/ZSM-35 ($x = 0, 1, 2$) samples, as shown in Fig. 2D. It can be seen that $\ln A$ and E_a exhibit excellent linear correlation, with $\ln A = mE_a + C$(where m is the proportionality constant and C is the constant at the intercept $E_a = 0$). This linear correlation has been reported previously, showing the so-called kinetic compensation effect of N_2O decomposition [21,27,28].

3.3. Concentrations of active Fe sites

The concentrations of active Fe sites in Fe/ZSM-35-HT samples were determined by the transient-response method. Fig. 3 presents the product-time profile after a step change from He flow to 5.0 vol% N_2O/He flow for the Fe/ZSM-35-HT ($x = 2$) catalyst at 523 K. N_2 appears immediately, but no oxygen is observed, indicating that only the reaction $N_2O + ()_{Fe} \rightarrow N_2 + (O)_{Fe}$ takes place. Thus, the concentrations of the active Fe sites are estimated based on the amount of N_2 evolved during N_2O decomposition [24,29] (Table 3). The percentage of the active Fe sites increases from 29% for Fe/ZSM-35-HT ($x = 0$) to 57% for Fe/ZSM-35-HT ($x = 1$), and further to 78% for Fe/ZSM-35-HT ($x = 2$), suggesting that introduced extra-framework Al is strongly related to the formation of active Fe sites for N_2O decomposition at low temperature. It should be mentioned that calcined catalysts show only negligible quantity of N_2 product under the same experimental conditions. The above results show that severe treatment is a prerequisite for the generation of active Fe sites [24,25,30].

3.4. UV–visible DRS of Fe/ZSM-35 catalysts

Fig. 4A displays the UV–visible DRS of both calcined and high-temperature-treated Fe/ZSM-35 catalysts. For the Fe/ZSM-35-C ($x = 0$) catalyst, three absorption bands centered at 275, 355, and 540 nm appear. With the increase in the quantity of extra-framework Al species, the intensities of the bands at 275 and 355 nm increase, accompanied by a decrease in the intensity of the band at around 540 nm. Treatment of the catalysts in helium at 1173 K leads to a dramatic reduction in the intensities of the bands at 275 and 355 nm, implying profound changes in the iron species upon high-temperature treatment. According to reports in the literature, the absorption bands below 300 nm [31–33] are assigned to isolated iron ions in tetrahedral or octahedral coordination, bands between 300 and 400 nm to small oligomeric Fe_xO_y clusters

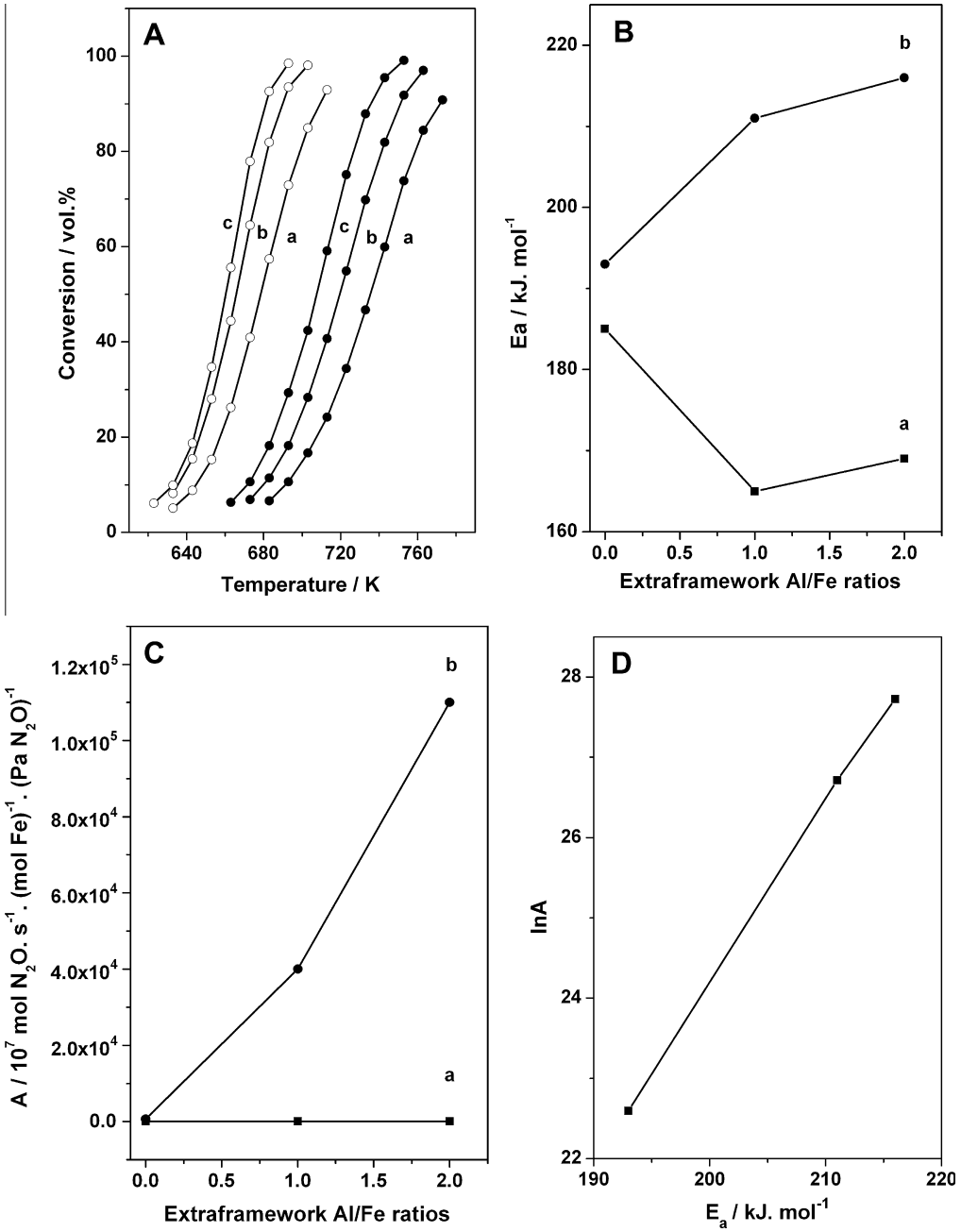

Fig. 2. (A) N_2O conversion as a function of reaction temperature over (a) (●, ○) Fe/ZSM-35 ($x = 0$); (b) (●, ○) Fe/ZSM-35 ($x = 1$); (c) (●, ○) Fe/ZSM-35 ($x = 2$). Solid symbols: calcined in O_2 at 823 K; open symbols: pretreated in He at 1173 K. Feedstock composition: 5.0 vol% N_2O in He. Dependence of (B) apparent activation energy and (C) pre-exponential factors on extra-framework Al/Fe ratios for Fe/ZSM-35 ($x = 0, 1, 2$) samples (a) calcined in O_2 at 823 K, (b) pretreated in helium at 1173 K. (D) ln$A$ versus E_a for N_2O decomposition of the high-temperature-treated Fe/ZSM-35 ($x = 0, 1, 2$) samples.

Table 2
First-order rate constants, apparent activation energies, and pre-exponential factors of high-temperature-treated Fe/ZSM-35 catalysts for N_2O decomposition.

Catalyst	First-order rate constant[c] (10^{-6} mol N_2O s^{-1} (mol Fe)$^{-1}$(Pa N_2O)$^{-1}$)	E_a[a] (kJ mol^{-1})	A[b] (10^{-7} mol N_2O s^{-1}(mol Fe)$^{-1}$(Pa N_2O)$^{-1}$)
Fe/ZSM-35-C ($x = 0$)	1.1	185	14
Fe/ZSM-35-C ($x = 1$)	1.8	165	1.0
Fe/ZSM-35-C ($x = 2$)	2.9	169	2.7
Fe/ZSM-35-HT ($x = 0$)	9.3	193	6.5×10^2
Fe/ZSM-35-HT ($x = 1$)	13	211	4.0×10^4
Fe/ZSM-35-HT ($x = 2$)	15	216	1.1×10^5

Notes: C: Calcined at 823 K in O_2 flow. HT: treated at 1173 K in helium flow.
[a] Apparent activation energy.
[b] Apparent pre-exponential factors.
[c] First-order rate constants calculated at 683 K.

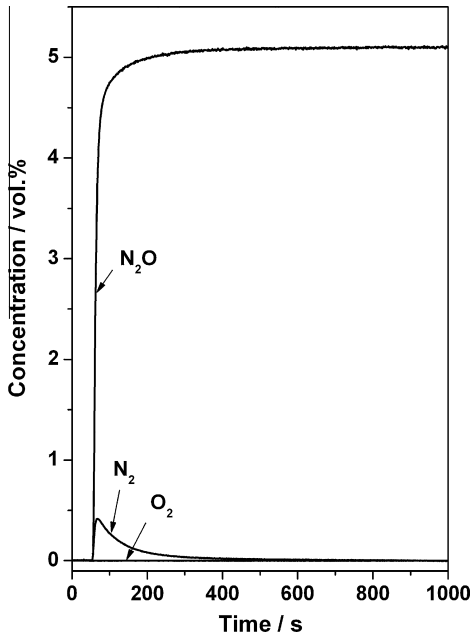

Fig. 3. Response to a step change from He flow to N_2O/He (5.0 vol%) flow on Fe/ZSM-35-HT ($x = 2$) sample.

Table 3
The number of active Fe sites determined by the transient-response method for the high-temperature-treated Fe/ZSM-35 ($x = 0, 1, 2$) samples.

Catalyst	N_2O decomposition	
	[active Fe sites] ($\times 10^{19}$ sites g^{-1})	O/Fe_{total}
Fe/ZSM-35-HT ($x = 0$)	3.5	0.29
Fe/ZSM-35-HT ($x = 1$)	5.4	0.57
Fe/ZSM-35-HT ($x = 2$)	7.8	0.78

[31,34], and bands above 400 nm to large Fe_2O_3 particles [20,21,35–38]. Alternatively, isolated Fe ions in octahedral coordination in Al_2O_3 give an absorption band at 286 nm, and binuclear Fe clusters also contribute to the absorption features in the region of 300–400 nm [9,20,39,40]. Thus, the absorption band at 275 nm can be ascribed to octahedrally coordinated Fe ions in close interaction with Al species, the band at 355 nm to oxygen-to-iron charge transfer transition of bi- and oligonuclear Fe clusters, and the band at 540 nm to large Fe_xO_y particles.

Deconvolution of the UV–visible absorbance bands into Gaussian subbands, followed by multiplication of the percentage of the subbands with respect to the total area of the experimental spectrum by the total iron content [36,41] gives the percentages of different Fe species (Table 4 and Fig. S1). This quantification does not account for the dependence of the extinction coefficient on the wavelength [41], but nevertheless provides a semiquantitative estimate of the distribution of the various Fe species. With an increase in the quantity of the extra-framework Al species, the percentage of bulky iron oxide aggregates decreases, while those of isolated iron species and bi- and oligonuclear Fe species increase, suggesting that introduction of extra-framework Al is beneficial for the formation and stabilization of mono-, bi-, and oligonuclear Fe species for both the calcined and high-temperature-activated catalysts.

3.5. IR spectra of adsorbed NO on Fe/ZSM-35 catalysts

IR spectroscopic study of NO adsorption has been applied to probe the active sites in Fe/ZSM-35 catalysts [1,10,15,17,42]. IR spectra of adsorbed NO on calcined Fe/ZSM-35 ($x = 0, 1, 2$) catalysts are presented in Fig. 5A. It can be seen that NO adsorption on Fe/ZSM-35 ($x = 0$) gives a characteristic IR band at 1620 cm^{-1} with a shoulder band at 1580 cm^{-1}. With increasing amounts of extra-framework Al species, the feature IR band at 1620 cm^{-1} becomes stronger, while the shoulder band at 1580 cm^{-1} does not show noticeable changes. According to the literature data, the band at 1620 cm^{-1} is attributed to linearly adsorbed NO_2 on iron ions [43–46], which is possibly due to NO_2 impurity in the NO probe gas or may arise from the interaction of adsorbed NO with residual oxygen species or extra-framework oxygen species. Additionally, the feature band observed at 1580 cm^{-1} belongs to monodentate/bidentate nitrate groups on iron sites [44,47–49].

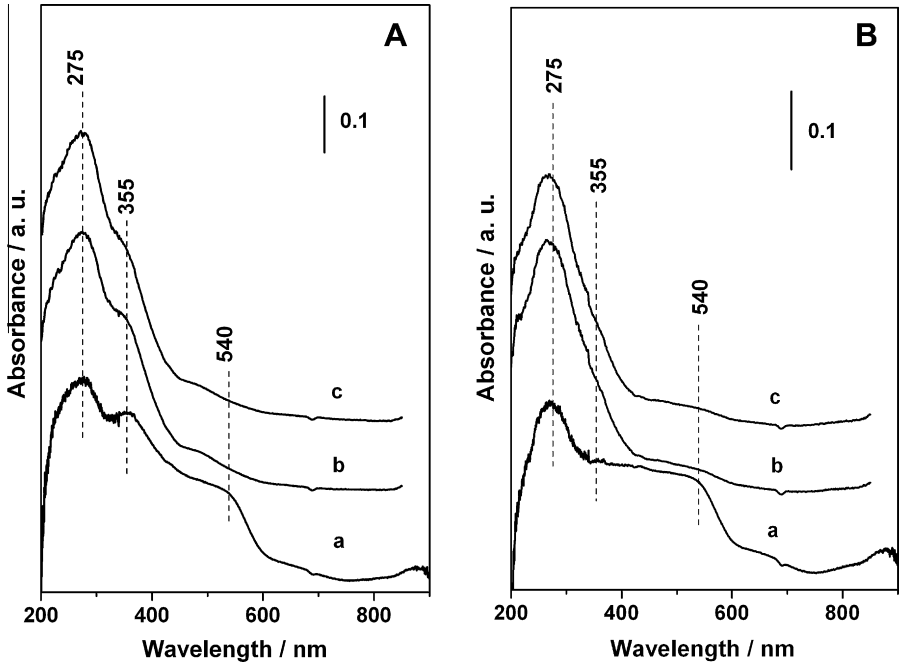

Fig. 4. UV–visible diffuse reflectance spectra of Fe/ZSM-35 samples (A) calcined in O_2 at 823 K and (B) treated in He at 1173 K: (a) Fe/ZSM-35 ($x = 0$), (b) Fe/ZSM-35 ($x = 1$), (c) Fe/ZSM-35 ($x = 2$).

Table 4
Percentages of different iron species calculated from the deconvolution of UV–visible diffuse reflectance spectra of Fe/ZSM-35 catalysts (Fig. 4).

Catalyst	Fe[a]		Fe[b]		Fe[c]	
	I_1	wt.%	I_2	wt.%	I_3	wt.%
Fe/ZSM-35-C (x = 0)	0.38	0.42	0.29	0.31	0.33	0.37
Fe/ZSM-35-C (x = 1)	0.54	0.59	0.36	0.40	0.10	0.11
Fe/ZSM-35-C (x = 2)	0.66	0.72	0.26	0.30	0.08	0.08
Fe/ZSM-35-HT (x = 0)	0.28	0.31	0.39	0.43	0.33	0.36
Fe/ZSM-35-HT (x = 1)	0.67	0.73	0.73	0.25	0.11	0.12
Fe/ZSM-35-HT (x = 2)	0.70	0.77	0.77	0.22	0.10	0.11

Notes: I_1: $\lambda < 300$ nm, I_2: $300 < \lambda < 450$ nm, I_3: $\lambda > 450$ nm. C: Calcined at 823 K in O_2 flow. HT: treated at 1173 K in helium flow.
[a] Isolated iron species in tetrahedra and octahedra.
[b] Oligonuclear iron clusters ($x \geqslant 2$).
[c] Bulk iron oxides.

High-temperature or steam treatment of the calcined catalysts can lead to an alteration of the structure of the active Fe sites [50,51] and extensive extraction of Al species from framework to extra-framework positions (Table 1). The extra-framework Al species can interact with the iron oxide clusters initially accommodated in the cationic exchange sites of the zeolite to form Fe–O–Al clusters. Fig. 5B exhibits the IR spectra of adsorbed NO on high-temperature-activated Fe/ZSM-35 ($x = 0$, 1, 2) catalysts. Fe/ZSM-35-HT ($x = 0$) shows strong IR bands at 1874 and 1626 cm^{-1} with a weak shoulder at 1645 cm^{-1}. Increasing amounts of introduced extra-framework Al species result in an increase in intensity of all three feature IR bands. Based on numerous studies of NO adsorption onto Fe-containing zeolite catalysts, we ascribe the shoulder band at 1645 cm^{-1} to NO_2 interacting with structural defects of the zeolite [47] and the IR band at 1874 cm^{-1} to adsorbed NO on clustered extra-framework Fe–O–Al mixed oxide species in zeolite micropores [44,48,49,52]. Compared to the Fe/ZSM-35-HT ($x = 0$) sample, intensity of the IR band at 1874 cm^{-1} increases for Fe/ZSM-35-HT ($x = 1$, 2) samples. ^{29}Si MAS NMR spectra show that the amount of extracted framework Al for the samples upon high-temperature treatment is almost the same (Table 1). Thus, the substantial differences in the 1874 cm^{-1} signal for Fe/ZSM-35-HT samples suggest that not every extracted framework Al can participate in the formation of active iron sites. In contrast, the introduced extra-framework Al is more beneficial for the formation of active iron sites.

3.6. UV Raman spectra of Fe/ZSM-35 catalysts

UV Raman spectra of both calcined and high-temperature-activated Fe/ZSM-35 ($x = 0$, 1, 2) catalysts are shown in Fig. 6. Except for the observation of the characteristic bands of ZSM-35 zeolite at 325, 425, and 800 cm^{-1} [48,53,54], a weak Raman band at 875 cm^{-1} and a broad band at 1165 cm^{-1} are observed for the calcined catalysts (Fig. 6A). After the calcined catalysts are treated at 1173 K in helium, some dramatic changes take place in the Raman spectra: the intensity of the Raman band at 875 cm^{-1} grows remarkably and the intensity of the Raman band at 1165 cm^{-1} decreases considerably (Fig. 6B). The feature Raman bands at 875 and 1165 cm^{-1} are not detected for the Al/ZSM-35 catalyst (not shown). The intense Raman band at 875 cm^{-1} has been assigned to binuclear Fe sites [12] and the band at 1165 cm^{-1} stems from the asymmetric stretching vibrations of isolated Fe–O–Si species in extra-framework or in framework positions [55–57]. It is very interesting that the intensity of the strong Raman band at 875 cm^{-1} increases with increased amounts of extra-framework Al species, reflecting the binuclear Fe sites probably being stabilized by extra-framework Al species on the high-temperature-activated catalysts. Fig. 6C presents the rate of N_2O decomposition versus the intensity ratio of the Raman band at 875 cm^{-1} to that at 425 cm^{-1}. The rate of N_2O decomposition increases with increasing intensity ratio of the Raman band at 875 cm^{-1} to that at 425 cm^{-1}. Such strong correlation suggests that the binuclear Fe sites bound to extra-framework Al species, characterized by the Raman band at 875 cm^{-1}, are the active sites for direct N_2O decomposition on the high-temperature treated catalysts.

3.7. ^{57}Fe Mössbauer spectra of high-temperature treated Fe/ZSM-35 catalysts

^{57}Fe Mössbauer spectroscopy is an ideal tool to study the oxidation state and coordination of iron species due to its high sensitivity to various iron species [16,25,58–61]. The Mössbauer spectra of

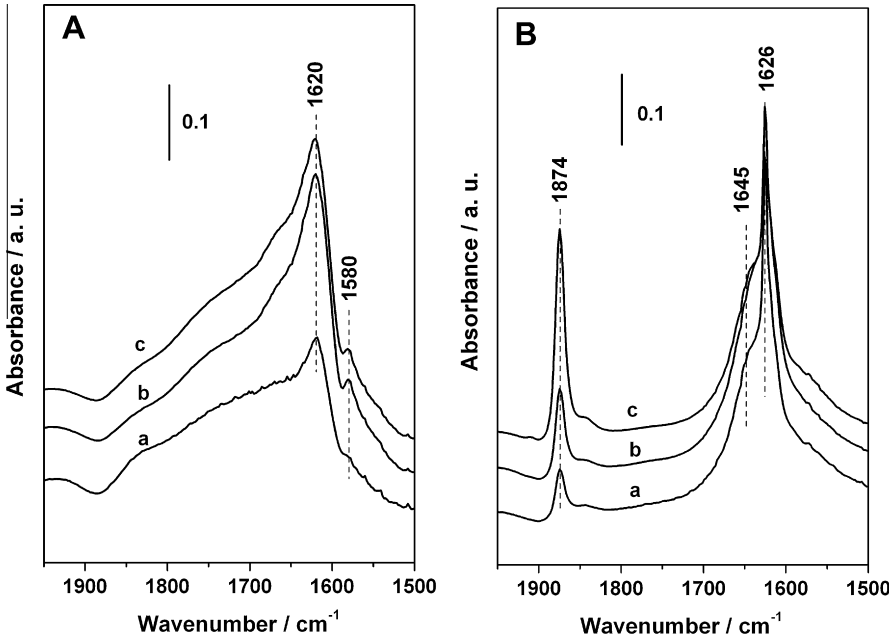

Fig. 5. IR spectra in the region 1500–1950 cm^{-1} recorded in situ after exposure of Fe/ZSM-35 catalysts to NO and then purging with N_2 for 10 min (A) calcined in O_2 at 823 K and (B) treated in He at 1173 K: (a) Fe/ZSM-35 ($x = 0$), (b) Fe/ZSM-35 ($x = 1$), (c) Fe/ZSM-35 ($x = 2$).

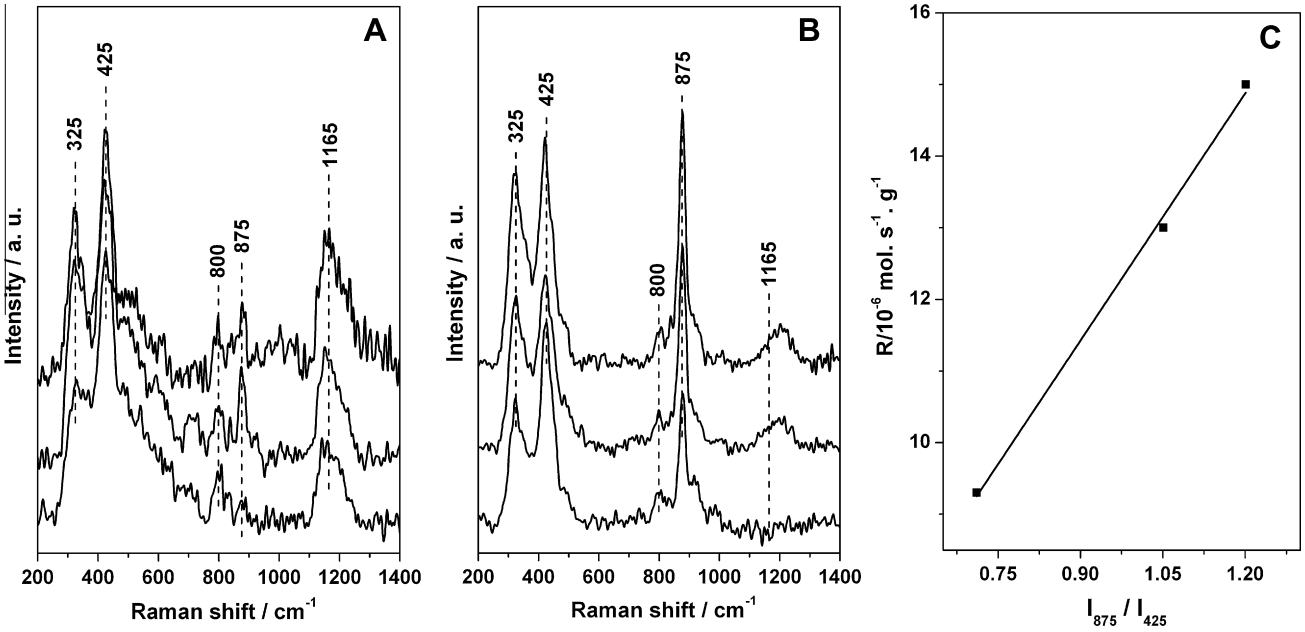

Fig. 6. UV Raman spectra recorded in situ of Fe/ZSM-35 catalysts (A) calcined in O_2 at 823 K and (B) treated in He at 1173 K: (a) Fe/ZSM-35 ($x = 0$), (b) Fe/ZSM-35 ($x = 1$), (c) Fe/ZSM-35 ($x = 2$). The excitation laser line is at 325 nm. (C) Dependence of the rate of N_2O decomposition at 683 K on the intensity ratio of the band at 875 cm^{-1} to that at 425 cm^{-1} for the high-temperature-treated catalysts.

the Fe/ZSM-35-HT ($x = 0, 1, 2$) catalysts recorded at 78 K are shown in Fig. 7 and the Mössbauer parameters are summarized in Table 5. According to the literature data, the components characterized by the parameters IS = 0.44 mm s^{-1}, QS = 0.32 mm s^{-1}, and magnetic field = 53.7 T and IS = 0.47 mm s^{-1}, QS = 0.36 mm s^{-1}, and magnetic field = 53.6 T correspond to α-Fe_2O_3 [58]. The two components described by IS = 1.29–1.32 mm s^{-1}, QS = 2.84–3.01 mm s^{-1}, and IS = 0.32–0.55 mm s^{-1}, QS = 1.01–1.14 mm s^{-1} are assigned to μ-oxo bridged binuclear Fe^{2+} complexes and mono-(μ-oxo) dimeric Fe^{3+} complexes, respectively [25]. One may notice that the spectral contribution of the high-spin mono-(μ-oxo) binuclear Fe^{2+} sites increases while that of the high-spin mono-(μ-oxo) binuclear Fe^{3+} sites decreases with increasing extra-framework Al content. It has been shown [52,62–64] that extra-framework iron species, in particular the bi- and oligonuclear Fe clusters, are able to undergo self-reduction upon high-temperature treatment under an inert atmosphere or vacuum. From earlier work, we also know that the presence of Al species promotes the reduction in Fe^{3+} ions to Fe^{2+} ions, especially bi- and oligonuclear iron clusters [65]. The present results indicate that the presence of extra-framework Al species and high-temperature treatment might be able to synergetically promote the autoreduction in the binuclear active Fe sites.

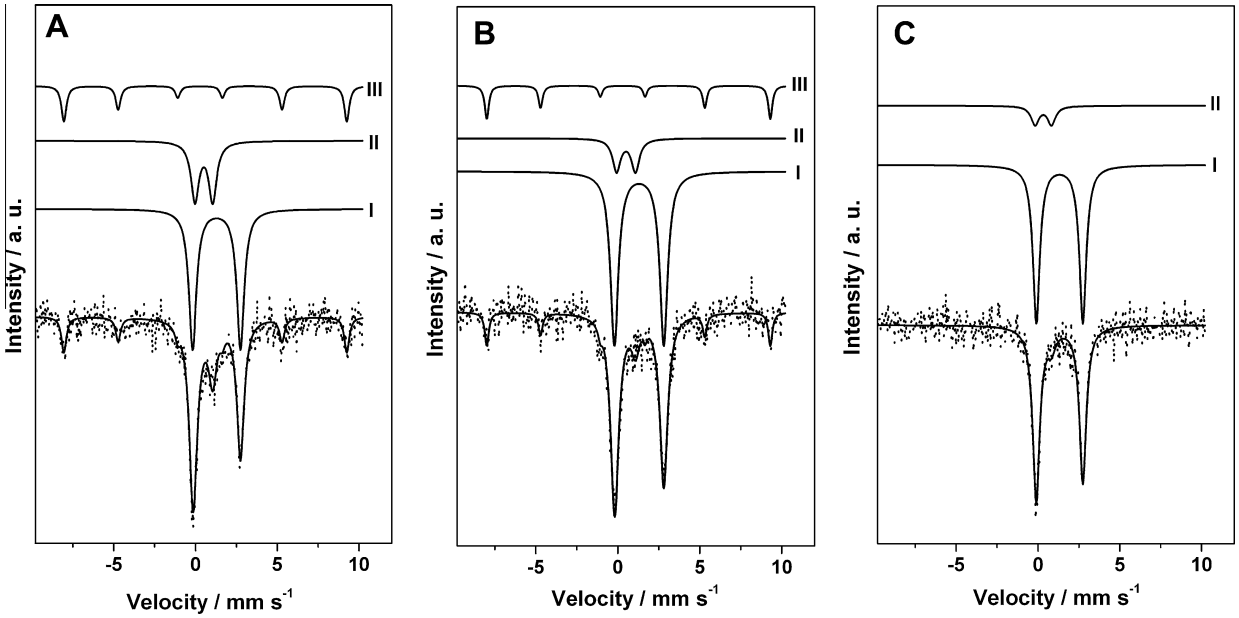

Fig. 7. 78 K ^{57}Fe Mössbauer spectra of high-temperature-activated Fe/ZSM-35 catalysts: (A) Fe/ZSM-35 ($x = 0$), (B) Fe/ZSM-35 ($x = 1$), (C) Fe/ZSM-35 ($x = 2$) at 78 K. The solid lines overlaid with the experimental spectra are least-squares fits to the raw data. The subspectra are shown above the experimental spectra as solid lines.

Table 5
^{57}Fe Mössbauer parameters of high-temperature-treated Fe/ZSM-35 catalysts at 78 K (Fig. 7).

Catalyst	Isomer shift[a] (mm s^{-1})	Quadruple splitting[b] (mm s^{-1})	Magnetic field (T)	Spectral contribution[c] (%)	FWHM[d] (mm s^{-1})	Subspectra and Fe sites
Fe/ZSM-35-HT (x = 0)	1.29	2.92		56.1	0.55	I. Fe^{2+}–O–Fe^{2+}
	0.51	1.09		25.3	0.58	II. Fe^{3+}–O–Fe^{3+}
	0.44	0.32	53.7	18.6	0.36	III. α-Fe_2O_3
Fe/ZSM-35-HT (x = 1)	1.3	3.01		72.4	0.58	I. Fe^{2+}–O–Fe^{2+}
	0.5	1.14		13.7	0.58	II. Fe^{3+}–O–Fe^{3+}
	0.47	0.36	53.6	14.0	0.29	III. α-Fe_2O_3
Fe/ZSM-35-HT (x = 2)	1.32	2.84		88.1	0.51	I. Fe^{2+}–O–Fe^{2+}
	0.32	1.01		11.9	0.58	II. Fe^{3+}–O–Fe^{3+}

[a] Isomer shift, relative to α-Fe at room temperature.
[b] Quadrupole splitting, electric quadrupole splitting.
[c] Relative resonance areas of the different components of the absorption patterns.
[d] Full line width at half maximum: uncertainty is ±5% of the reported values.

Overall, our experimental results point to a strong synergetic effect between extra-framework Fe species and Al species in N_2O decomposition. A common sense understanding is that high-temperature treatment is required to form active Fe sites [20,66]. Recently, several works [6,14] have provided strong evidence that Al species are a necessary component in the generation of the active Fe sites in Fe/ZSM-35 catalysts. This work provides some further insight into this issue. Our ^{29}Si MAS NMR spectra indicate substantial dislodgement of framework Al upon high-temperature treatment for the calcined catalysts (Fig. 1 and Table 1). IR spectra of NO adsorption provides additional support for the stabilization of the active Fe sites by forming an extra-framework Fe–O–Al mixed oxide phase (IR band at 1874 cm^{-1}) in Fe/ZSM-35-HT (x = 0, 1, 2) catalysts. UV–visible DRS, UV Raman spectra, and ^{57}Fe Mössbauer spectra results suggest significant modifications in the structure of isolated and bi- and oligonuclear Fe species upon high-temperature activation and introduction of extra-framework Al species. Based on these comprehensive spectroscopic results and the activity measurements, it is concluded that the newly formed binuclear active Fe sites with feature Raman band at 875 cm^{-1} are responsible for the catalytic N_2O decomposition in Fe/ZSM-35-HT (x = 0, 1, 2) catalysts. High-temperature activation and the presence of extra-framework Al species are beneficial for both the formation and the reduction in such binuclear active Fe sites stabilized by extra-framework Al species.

4. Conclusions

The effect of extra-framework Al via $AlCl_3$ deposition on structure of the active Fe sites of Fe/ZSM-35 catalysts and the catalytic activities in N_2O decomposition has been investigated. The N_2O conversion increases with increasing extra-framework Al content for both the calcined and high-temperature-treated Fe/ZSM-35 catalysts. High-temperature treatment profoundly changes the iron speciation. UV–visible DRS and IR spectra of NO adsorption results show that a considerable fraction of clustered and cationic Fe species are transformed into extra-framework Fe–O–Al mixed oxide species upon high-temperature treatment. UV Raman spectra and ^{57}Fe Mössbauer spectra (^{57}Fe Mössbauer parameters IS = 1.29–1.32 mm s^{-1}, QS = 2.84–3.01 mm s^{-1}) indicate the formation of binuclear Fe sites stabilized by extra-framework Al species with a feature Raman band at 875 cm^{-1}, which are responsible for the high activity of N_2O decomposition. The possible explanation is that the addition of extra-framework Al species is beneficial for the formation and reduction in the binuclear active Fe sites bound to extra-framework Al species. This work sheds light on the nature of the active Fe sites and the function of extra-framework Al species in enhancing the catalytic performance of Fe/ZSM-35 catalysts.

Acknowledgments

The authors are grateful to the Program Strategic Scientific Alliances between China and the Netherlands (Grant 2008DFB50130), the National Basic Research Program of China or 973 Program (Grant 2009CB623507), and the National Natural Science Foundation of China (NSFC, No. 21003122) for financial support.

Appendix A. Supplementary material

Supplementary data associated with this article can be found, in the online version, at http://dx.doi.org/10.1016/j.jcat.2013.01.011.

References

[1] I. Malpartida, E. Ivanova, M. Mihaylov, K. Hadjiivanov, V. Blasin-Aubé, O. Marie, M. Daturi, Catal. Today 149 (2010) 295.
[2] J. Nováková, Z. Sobalík, Catal. Lett. 127 (2009) 95.
[3] S.S. Shevade, B.S. Rao, Catal. Lett. 66 (2000) 99.
[4] K. Jíša, J. Nováková, M. Schwarze, A. Vondrová, S. Sklenák, Z. Sobalík, J. Catal. 262 (2009) 27.
[5] J. Nováková, M. Schwarze, Z. Sobalík, Catal. Lett. 104 (2005) 157.
[6] J. Dděček, L. Čapek, P. Sazama, Z. Sobalík, B. Wichterlová, Appl. Catal. A 391 (2011) 244.
[7] J. Nováková, M. Lhotka, Z. Tvarůžková, Z. Sobalík, Catal. Lett. 83 (2002) 215.
[8] J. Nováková, Z. Sobalík, Catal. Lett. 111 (2006) 195.
[9] S. Sklenak, P.C. Andrikopoulos, B. Boekfa, B. Jansang, J. Nováková, L. Benco, T. Bucko, J. Hafner, J. Dděček, Z. Sobalík, J. Catal. 272 (2010) 262.
[10] V. Blasin-Aubé, O. Marie, J. Saussey, A. Plesniar, M. Daturi, N. Nguyen, C. Hamon, M. Mihaylov, E. Ivanova, K. Hadjiivanov, J. Phys. Chem. C 113 (2009) 8387.
[11] N.A. Kachurovskaya, G.M. Zhidomirov, R.A. van Santen, J. Phys. Chem. B 108 (2004) 5944.
[12] We have identified the active iron site for N_2O decomposition as an $Fe_2(\mu$-O) site, characterized by a Raman band at 875 cm^{-1} by in situ UV resonance Raman spectroscopy combined with Mössbauer spectroscopy and DFT calculations. This is our previous work, submitted but unpublished.
[13] D. Kaucký, Z. Sobalík, M. Schwarze, A. Vondrová, B. Wichterlová, J. Catal. 238 (2006) 293.
[14] Z. Sobalík, J. Nováková, J. Dděček, N.K. Sathu, E. Tabor, P. Sazama, P. Stastny, B. Wichterlova, Micropor. Mesopor. Mater. 146 (2011) 172.
[15] L. Benco, T. Bucko, R. Grybos, J. Hafner, Z. Sobalík, J. Dděček, S. Sklenak, J. Hrusak, J. Phys. Chem. C 111 (2007) 9393.
[16] E. Tabor, K. Závta, N.K. Sathu, A. Vondrová, P. Sazama, Z. Sobalík, Catal. Today 175 (2011) 238.
[17] E. Ivanova, M. Mihaylov, K. Hadjiivanov, V. Blasin-Aubé, O. Marie, A. Plesniar, M. Daturi, Appl. Catal. B 93 (2010) 325.
[18] M.A. Uddin, T. Komatsu, T. Yashima, J. Catal. 150 (1994) 439.
[19] R.Q. Long, R.T. Yang, Chem. Commun. 17 (2000) 1651.
[20] K. Sun, H. Xia, Z. Feng, R.A. van Santen, E.J.M. Hensen, C. Li, J. Catal. 254 (2008) 383.
[21] H. Xia, K. Sun, F. Fan, K. Sun, W. Su, Z. Feng, P. Ying, C. Li, J. Catal. 259 (2008) 269.
[22] B. Sulikowski, J. Find, H.G. Karge, D. Herein, Zeolite 19 (1997) 395.
[23] C. Jia, P. Beaunier, P. Massiani, Micropor. Mesopor. Mater. 24 (1998) 69.
[24] L. Kiwi-Minsker, D.A. Bulushev, A. Renken, J. Catal. 219 (2003) 273.
[25] K.A. Dubkov, N.S. Ovanesyan, A.A. Shteinman, E.V. Starokon, G.I. Panov, J. Catal. 207 (2002) 341.

[26] X. Li, W. Zhang, S. Liu, L. Xu, X. Han, X. Bao, J. Catal. 250 (2007) 55.
[27] E.R.H. vanEck, J.A.Z. Pieterse, A.P.M. Kentgens, Solid State Nucl. Magn. Reson. 39 (2011) 99.
[28] G.C. Bond, M.A. Keane, H. Kral, J.A. Lercher, Catal. Rev. Sci. Eng. 42 (2000) 323.
[29] C.A. Fyfe, J.L. Bretherton, L.Y. Lam, J. Am. Chem. Soc. 123 (2001) 5285.
[30] J.L. Motz, H. Heinichen, W.F. Hölderich, J. Mol. Catal. A Chem. 136 (1998) 175.
[31] I. Yuranov, D.A. Bulushev, A. Renken, L. Kiwi-Minsker, J. Catal. 227 (2004) 138.
[32] G.I. Panov, CATTECH 4 (2000) 18.
[33] S. Bordiga, R. Buzzoni, F. Geobaldo, C. Lamberti, E. Giamello, A. Zecchina, G. Leofanti, G. Petrini, G. Tozzola, G. Vlaic, J. Catal. 158 (1996) 486.
[34] H.H. Tippins, Phys. Rev. B 1 (1970) 126.
[35] G. Lehmann, Z. Phys. Chem. 72 (1970) 279.
[36] M. Schwidder, M.S. Kumar, K. Klementiev, M.M. Pohl, A. Brückner, W. Grünert, J. Catal. 231 (2005) 314.
[37] G.D. Pirngruber, P.K. Roy, R. Prins, Phys. Chem. Chem. Phys. 8 (2006) 3939.
[38] J. Pérez-Ramírez, J.C. Groen, A. Brückner, M.S. Kumar, U. Bentrup, M.N. Debbagh, L.A. Villaescusa, J. Catal. 232 (2005) 318.
[39] M.S. Kumar, M. Schwidder, W. Grünert, A. Brückner, J. Catal. 227 (2004) 384.
[40] K. Sun, H. Xia, E.J.M. Hensen, R.A. van Santen, C. Li, J. Catal. 238 (2006) 186.
[41] D.M. Kurtz Jr., Chem. Rev. 90 (1990) 585.
[42] G. Centi, S. Perathoner, R. Arrigo, G. Giordano, A. Katovic, V. Pedulà, Appl. Catal. A 307 (2006) 30.
[43] J. Pérez-Ramírez, M.S. Kumar, A. Brückner, J. Catal. 223 (2004) 13.
[44] Z. Sobalík, K. Jíša, H. Jirglová, B. Bernauer, Catal. Today 126 (2007) 73.
[45] H. Chen, T. Voskoboinikov, W.M.H. Sachtler, J. Catal. 180 (1998) 171.
[46] L.J. Lobree, I. Hwang, J.A. Reimer, A.T. Bell, Catal. Lett. 63 (1999) 233.
[47] C.H. Rochester, S.A. Topham, J. Chem. Soc. Faraday Trans. 1 (1979) 872.
[48] M.D. Amiridis, F. Puglisi, J.A. Dumesic, W.S. Millman, N. Topsøe, J. Catal. 142 (1993) 572.
[49] E.J.M. Hensen, Q. Zhu, R.A. van Santen, J. Catal. 233 (2005) 136.
[50] G. Mul, J. Pérez-Ramírez, F. Kapteijn, J.A. Moulijn, Catal. Lett. 80 (2002) 129.
[51] H.-Y. Chen, El-M. El-Malki, X. Wang, R.A. van Santen, W.M.H. Sachtler, J. Mol. Catal. A Chem. 162 (2000) 159.
[52] E.J.M. Hensen, Q. Zhu, R.A. van Santen, J. Catal. 220 (2003) 260.
[53] Q. Zhu, E.J.M. Hensen, B.L. Mojet, J.H.M.C. van Wolput, R.A. van Santen, Chem. Commun. 11 (2002) 1232.
[54] L.J. Lobree, I.-C. Hwang, J.A. Reimer, A.T. Bell, J. Catal. 186 (1999) 242.
[55] P.K. Dutta, K.M. Rao, J.Y. Park, J. Phys. Chem. 95 (1991) 6654.
[56] P.K. Dutta, K.M. Rao, J.Y. Park, Langmuir 8 (1992) 722.
[57] K. Sun, F. Fan, H. Xia, Z. Feng, W.-X. Li, Can Li, J. Phys. Chem. C 112 (2008) 16036.
[58] C. Li, J. Catal. 216 (2003) 203.
[59] F. Fan, K. Sun, Z. Feng, H. Xia, B. Han, Y. Lian, P. Ying, Can Li, Chem. – Eur. J. 15 (2009) 3268.
[60] E. Tabor, K. Závta, N.K. Sathu, Z. Tvarůžková, Z. Sobalík, Catal. Today 169 (2011) 16.
[61] J.B. Taboada, E.J.M. Hensen, I.W.C.E. Arends, G. Mul, A.R. Overweg, Catal. Today 110 (2005) 221.
[62] K. Lázár, G. Lejeune, R.K. Ahedi, S.S. Shevade, A.N. Kotasthane, J. Phys. Chem. B 102 (1998) 4865.
[63] L. Guczi, K. Lázár, React. Kinet. Catal. Lett. 96 (2009) 335.
[64] R. Joyner, M. Stockenhuber, J. Phys. Chem. B 103 (1999) 5963.
[65] G.D. Pirngruber, P.K. Roy, R. Prins, J. Catal. 246 (2007) 147.
[66] T.V. Voskoboinikov, H.-Y. Chen, W.M.H. Sachtler, Appl. Catal. B 19 (1998) 279.